International Journal of Engineering & Technology, 7 (4.18) (2018) 390-399

International Journal of Engineering & Technology

Website: www.sciencepubco.com/index.php/IJET

Research paper

Characterization of Sand Proppant and Its Improvement via Polyurethane Coating

Noor Fitrah Abu Bakar[1*], Siti Norhidayah Abdullah Zawawi[1], Rohani Mohd Zin[1*], Norazah Abdul Rahman[1], Norin Zamiah Kassim Shaari[1]

[1]Faculty of Chemical Engineering, Universiti Teknologi MARA (UiTM), 40450 Shah Alam, Selangor, Malaysia
**Corresponding author E-mail: fitrah@salam.uitm.edu.my; rohanimz@salam.uitm.edu.my*

Abstract

Characterization of sand as proppant, its improvement using a simple polyurethane coating technique without heating and its coating evaluation using impingement test were investigated. Sand samples were obtained from eight locations in Malaysia beaches. Several important properties of proppant namely particle size distribution, density, turbidity, acid solubility, roundness and sphericity, and crush resistance were determined. Sample from Pantai Bachok, Kelantan showed the best characteristics of proppant that complies with the specifications set by API and ISO except for acid solubility and crush resistance. The proppant sample size of 20/40 mesh size was with density of 1.67g/cm^3, turbidity of 162 FTU, acid solubility of 2.8%, roundness and sphericity of 0.46 and 0.7, respectively. For crush testing, all sand samples can only withstand pressure up to 2000 psi. Polyurethane (PU) formulated from palm oil-based polyols has been used to coat the sand particles to improve acid solubility and crush resistance of the beach sand. The PU-coated sands from Pantai Bachok, Kelantan showed better acid solubility of only 0.38% and crush resistance of approximately 10% at 4000 psi than the uncoated ones. The impingement test showed that PU-coated sands gave less impact towards metal target and lower metal losses.

***Keywords*:** *proppant; sand; polyurethane coating; impingement; Malaysia coasts.*

1. Introduction

Propping agent or proppant [1-4] is an aid material used in hydraulic fracturing [5-7] process for the extraction of oil and gas from reservoir by keeping the created fracture open. Proppants are small particle used in combination with fracturing fluid and it is the second abundant constitute in a typical fracturing fluid with composition of 9.5 wt% [8]. It can be classified in two categories namely conventional and advanced types. Conventional proppants include sand, ceramic, nutshells and glass beads while proppant that are coated with polymer are known as advanced proppant. Currently, there are three types of proppant used namely sand, ceramic and resin-coated proppant (RCP) that comprised 80%, 10% and 10% by volume, respectively. [9-11]

Since the ideal proppant properties should have the traits of highly resistant to acid and corrosion [12-15], high strength [16-19], and readily available at low cost [8], the oilfield developers tend to use sand proppant with some improvements. Although sand proppant is not strong enough to withstand high closure stresses [20] which it deteriorates rapidly when the stress exceeds approximately 6000 psi [11, 8], the sand proppant can resist acid attacks effectively because of its monocrystalline silicon and contains no glassy constituents [12].

Polymer/resin-coated proppant (RCP) has been developed [20-22] to improve the properties of conventional sand proppant. RCP has many benefits for the hydraulic fracturing operation [8]. Coated proppant comprised a substrate (i.e proppant) and a layer of polymer. Modification of surface properties of substrates is performed by means of polymer coating to obtain favorable effects such as improved surface topography, wettability, and chemical reactivity [21, 23]. The most common types of organic polymers for proppant coating are the different types of resins, furan [24] polyesters and vinyl esters [8].

Polyurethanes (PU) are the most versatile polymers used in foams, coatings and castings. PU can be formulated or tailored to meet a wide range of application by adding isocyanate and polyols or biopolyols [25]. By synthesizing PU from more renewable resources such as polyols from palm oil based, it gives strong impact to the ecological and economical standpoint especially in Malaysia whereby the current economic growth of the commodity crops is mainly from palm oil.

This study aims to improve the properties of Malaysia beach sand to fulfil the API specification for proppant through the coating with polyurethane (PU) formulated from palm oil-based polyols. This work is focused on the evaluation of PU coating for micron size particles at room temperature as a simple coating approach without heating to avoid the usage of extensive energy. It is hypothesized that the proppant conductivity under elevated temperature is bearable because PU formed using polyols and diisocyanate is widely known as thermosetting polymers which do not melt when heated. However, the conductivity study is not conducted due to the limitation of equipment. As an alternative, impingement testing is demonstrated to evaluate the impact of the PU coated sand proppant on metal surface. The test resembles the flow back condition that may cause severe erosion on the surface equipment during hydraulic fracturing process [22].

Copyright © 2018 Authors. This is an open access article distributed under the Creative Commons Attribution License, which permits unrestricted use, distribution, and reproduction in any medium, provided the original work is properly cited.

2. Methodology

2.1. Characterization of sand samples

2.1.1 Materials and sample preparation

Sand samples were obtained from eight locations in Malaysia; three from West Coastal beaches (Selangor) and five from East Coastal beaches (Kelantan). All samples were properly washed and dried before further characterizations. The samples are noted as in Table 2.

1.1.2 Mineralogy and chemical composition analysis

In order to provide an understanding of overall mineralogy and chemical compositions such as quartz, alumina, graphite and CaO of sand samples, an analysis using X-Ray Diffraction (XRD) and X-Ray Fluorescence (XRF) were conducted.

(a) X-Ray Diffraction

X-Ray pattern of sand samples were recorded with a Rigaku X-Ray generator operating at 40kV and 30mA using CuKα wavelength of 1.5406 Å. An exposed time of 1 hour was used with step size of 1°/min ranging from 15º - 75º. Prior to the measurement, the sand sample was crushed using mortar and compacted into a pestle shape.

(b) X-Ray Fluorescence

Chemical compositions of sand samples such as SiO_2, Al_2O_3, Fe_2O_3 were examined using PANalytical X-Ray Fluorescence. 10 grams of sample was crushed and pressed under a pressure of 1000 psi to form into pellets. The pressed pellets were dried at 60 °C for one day in an oven to be further analyzed.

1.1.3 API and ISO standard for proppant characterization

Testing specifications for the sand proppants used in this study were conducted based on the International Organization for Standardization (ISO) and American Petroleum Institute (API) recommendations [24, 26-28].

(a) *Particle size distribution*

A series of stacked, wire-mesh sieves of standard sizes from 106 to 1250 µm were used to sieve all sand samples. 200g of sample was placed on the top sieve tray. Then, the sample was vibrated using a sieve shaker for 10 minutes. The amount of sample passed and retained on the sieve tray was weighed and recorded.

(b) *Bulk density*

The value of bulk density was obtained by measuring the weight of sand that was placed in a 100 ml measuring cylinder. Bulk density was calculated by dividing the mass of sand to the total volume of sand.

(c) Turbidity

Turbidity was measured by using a turbidimeter, where 5 g of sample and 15 ml of distilled water were added into the turbidity cell. The cell was then capped and shaken vigorously for approximately 30 s to suspend the sand particles.

(d) Acid solubility

To evaluate the acid solubility for sand, 5 g of sand was placed in 100 ml acid solution for 30 minutes at 150 °F (66 °C). The acid solution was prepared using 12 wt% of 3.5 M hydrochloric acid (HCl) and 3 wt% of 1.5 M of hydrofluoric acid (HF). Then, the residual sands were filtered and dried. Mass of sand before and after the acid treatment was recorded and acid solubility was calculated by using Eq. (1).

$$Acid\ solubility\ (\%) = \frac{m_{initial} - m_{final}}{m_{initial}} x\ 100 \quad (1)$$

Where

$m_{initial}$ = mass of sand before acid treatment (g)

m_{final} = mass of sand after acid treatment (g)

(e) Roundness and sphericity

Roundness and sphericity of sand were determined by visual-manual comparison of sand particles under microscope with magnification of 10 times. 20 particles were randomly examined and the images from microscope were then compared with the Krumbein and Sloss Chart [29]. The average sphericity and roundness of the samples were recorded.

(f) Crush resistance test

For crush resistance test, 15 g of sieved sand was filled into crush cell and stress level of 500, 1000, 1500, 2000 and 2500 psi were applied for 2 minutes. Crushed sand was then sieved and weighed to calculate the percentage of crushed sand / fines by using Eq. (2).

$$Crush\ value(\%) = \frac{m_{fines}}{m_{coarse}} x\ 100 \quad (2)$$

Where

m_{fines} = mass of sand after crush / mass of fines produced (g)

m_{coarse} = mass of sand before crush (g)

2.2. Coating of sand using Polyurethane (PU)

2.2.1 Materials

Palm oil based polyols was obtained from Malaysian Palm Oil Board (MPOB) Bangi, Selangor, Malaysia. Other materials include Methylene diphenyl diisocyanate (MDI) (Merck, 820797), triethylene diamine (TEDA) (sigma Aldrich, D27802), stannous octoate (sigma Aldrich, S3252), polydimethylsiloxane (PDMS) (Sigma Aldrich, 433012) and diethanolamine (Merck, 803116). Distilled water was used as blowing agent

2.2.2 Preparation of Polyurethane (PU)

Formulation of PU used in this study is given in Table 1. The formulations consist of two main components namely MDI and polyol, and additives such as stannous octoate, TEDA, PDMS, diethanolamine and distilled water. TEDA is a strong multi-purpose gelling catalyst used in the reaction between polyol and isocyanate. Improved catalytic activity in the gelling reaction is achieved when TEDA is used in the combination with an organometallic catalyst such as stannous octoate. PDMS is a common surfactant and a component of defoamer, which is used to suppress the formation of foams while diethanolamine acts as a cross-linker and corrosion inhibitor.

Table 1: Formulation of polyurethane (PU) as proppant coating

Mass ratio of Polyol: MDI	Catalysts		PDMS	Diethanol amine	Distilled water
	Stannous Octoate	TEDA			
1:5	1 drop	1 drop	1 drop	1 drop	1 drop

The mass ratio of polyols to MDI in the preparation of PU was 1:5. First, 5 g of polyol was placed in 50 ml beaker. A drop of each catalyst (stannous octoate, TEDA, PDMS, diethanolamine) and distilled water were mixed with polyol. The mixture was stirred thoroughly using a spatula for 2 minutes to obtain a homogenous mixture. 25 g of MDI was added to the mixture and stirred for 10 seconds.

2.2.3 Preparation of Sand Coating

100 g of selected sand sample was placed on an aluminum sheet. The prepared polyurethane (PU) resin in section 2.2.2 was dropped on the sand and the particle was coated one by one by the PU. Then the sample was cured at room temperature for 24 hours.

2.2.4 Characterizations of polyurethane PU-coated sand

(a) *Fourier Transform Infrared (FTIR) Spectroscopy*
FTIR spectras in the wave number region of 4000–500 cm^{-1} were obtained using a Perkin-Elmer 1750 FTIR spectrometer. Sand samples were crushed using mortar before being examined. The spectrums were analyzed to check and confirm structures of resins.

(b) *Images analysis*
The surface of uncoated and PU-coated sand was observed using microscope under 10x magnification to evaluate the surface coating of the PU-coated sand.

(c) *API and ISO standard for PU-coated sand characterization.*
PU-coated sand was characterized using the same methods as in section 2.1.3 except for the crush resistance test. Eight different stress levels i.e. 500, 1000, 1500, 2000, 2500, 3000, 3500 and 4000 psi were applied on the samples.

(d) *Impingement test of PU-coated sands*
An experiment is conducted to address the erosive tendencies of uncoated and PU-coated sands by performing a series of impingement test. Air was fed through an acrylic pipe with inner diameter of 8 mm and 4 m length at gas velocity of 100 m/s. In this case, 250 grams of proppant i.e. PU-coated and uncoated sand were fed in compressed air stream and the samples were projected toward targeted metal i.e. mild steel with a 90° of impingement angle. Figure 1 shows an experimental setup of the impingement test.

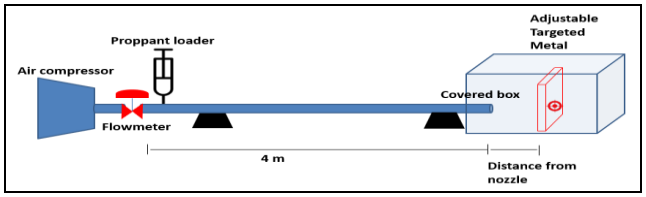

Fig. 1: Experimental Setup of Impingement Test

The tests were conducted at a different separation distance of 0.5, 2.5 and 5 inches of nozzle and target, at flowrate of 200 l/min (velocity of 100 m/s). The mass of targeted metal losses during the impingement operation was evaluated by weighing the metal. Images of the proppants impact on surface of targeted metal were captured by using a digital camera.

3. Results and discussion

3.1. Mineralogy and chemical composition of sand samples

Figure 2 shows XRD patterns for all sand samples. Generally, all samples showed similar mineralogical compositions. These patterns indicated characteristic peak of SiO_2[30-31], Fe_2O_3[32], Al_2O_3 [33], CaO [34], MgO [35], TiO_2 [30] and [36] as detailed in the Figure 2. The samples confirm the siliceous nature of Malaysia beach sands [37].
Table 2 shows chemical compositions for all sand samples namely SiO_2, FeO_3, Al_2O_3, CaO, MgO and K_2O that are quantified using XRF. The main compounds found in the sample were comparatively similar to the beach sand as in [38]. However, for Malaysia beach coast, SiO_2 is the major compound found in all samples which constitute more than 50%, followed by Fe_2O_3 and other oxides in trace amount. The amount of SiO_2 ranged from 49.8 to 76.5%. West Coast sand sample has higher percentage of SiO_2 ranging from 75.1-76.5% compared to East Coast with values of 49.8-70.9%. This is due to different geological rock structure between West and East coastal beaches [39].

Table 2: Chemical compositions of all sand samples

No	Sample	Composition (%)					
		SiO_2	Fe_2O_3	Al_2O_3	MgO	K_2O	CaO
1	Pantai Kelanang	76.54	17.12	3.82	0.97	1.17	0.37
2	Pantai Morib	75.27	16.32	5.39	1.89	1.04	0.10
3	Pantai Gold Coast	75.23	17.98	4.35	1.71	0.65	0.09
4	Pantai Kemasin	49.81	24.53	9.68	6.60	2.11	7.28
5	Pantai Bachok	66.02	19.70	8.51	2.30	2.45	1.02
6	Pantai Kubang Golok	61.09	21.65	5.75	2.36	1.80	7.37
7	Pantai Cahaya Bulan	69.04	18.63	7.45	1.43	2.37	1.09
8	Pantai Sabak	70.99	18.36	6.80	1.28	2.03	0.54

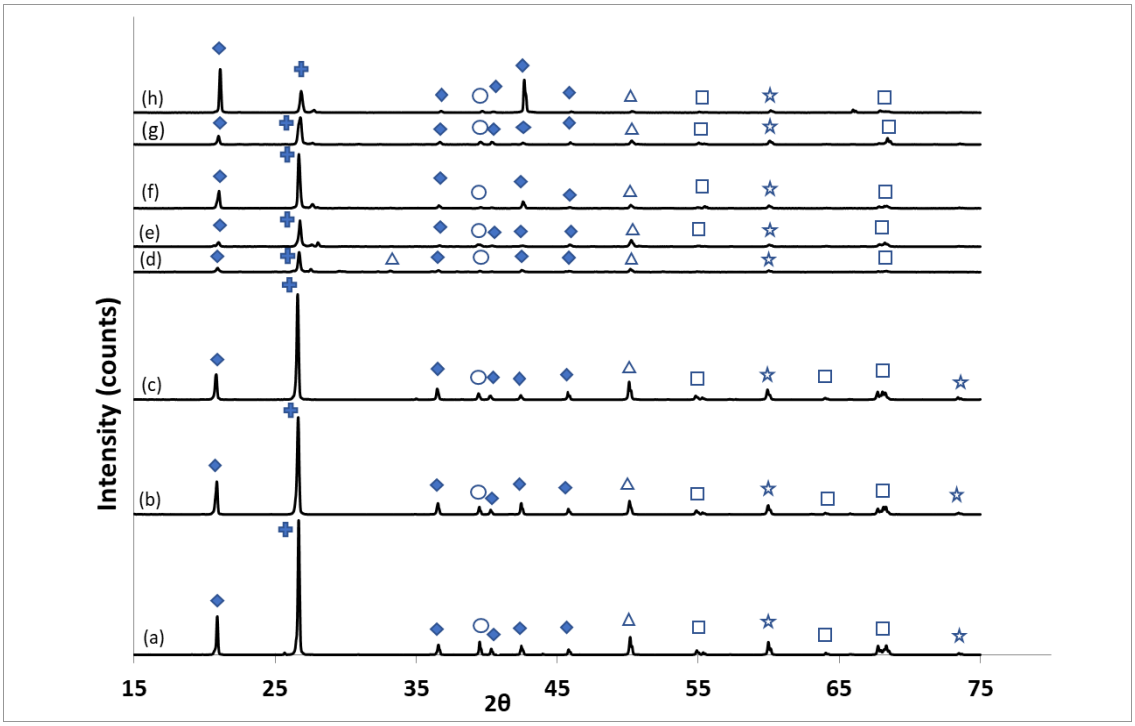

Fig. 2: XRD results for sand samples from a) Pantai Kelanang, b) Pantai Morib, c) Pantai Gold Coast, d) Pantai Kemasin, e) Pantai Bachok, f) Pantai Kubang Golok, g) Pantai Cahaya Bulan, h) Pantai Sabak.

(SiO_2; TiO_2; Al_2O_3; Fe_2O_3; CaO; MgO)

3.2. Characterization of sand samples as proppant

Table 3 shows the size and percentage in size of all sand samples. Samples 2, 3 and 4 have the smallest particle size distribution which ranges from 106-212 µm with classification of 70/40 mesh size followed by sample 1 and 6 and the coarsest size of Sample 7 and 8 with mesh size of 40/70 and 20/40 respectively. From Table 3, all samples comply with API standards that 90% of sample retains within the size class designation [24, 29]. Study by Zdunczyk 2007 [29] stated that 20/40 is the most widely used size fraction and sand samples from Sample 5, 7 and 8 fulfil the size fraction.

Figure 3 shows the particle size distribution for all sand samples. Sands from West Coast beaches are mostly fine and narrow in size with an average size of 120-130 µm except for Sample 1 with an average size of approximately 250 µm. Meanwhile, sand from East Coast beaches are coarser and have a wide size distribution with an average size of 500 µm except for Sample 6 which has the average size of 250 µm.

Table 4 shows result for bulk density, turbidity, acid solubility, roundness and sphericity of all samples. The bulk density ranged from 1.40 to 1.67 g/cm^3. However, only Sample 1, 5, 7 and 8 are within the API standard for proppant density which must be greater than 1.5 g/cm^3. For turbidity measurement, recommended limit of tested sand must be less than 250 FTU [24, 27, 29]. All samples meet the turbidity requirement that is set by the ISO and API standards except for Sample 4, 7 and 8. From XRF analysis, these samples contained higher percentage of aluminum oxides (Al_2O_3) compared to others, ranging from 6.8 to 9.7% which lead to high turbidity.

Acid solubility shows the amount of sand that is soluble in strong acid. It is an important characteristic for proppant to work effectively as acid treatment during completions of oil and gas wells is a common process in the hydraulic fracturing process [40]. API recommends the acid solubility to be no greater than 2% (by weight) for proppants of 6/12 to 30/50 mesh size and 3% (by weight) for proppants of 40/70 to 70/140 mesh size to be soluble in a 12:3 ratio of hydrochloric (HCl) to hydrofluoric (HF) acid solutions [24, 27, 29].

Table 3: Sample sieve analysis results

No	Name of Beaches	Size classes		In size (%)
		Mesh size	Size, µm	
1	Pantai Kelanang	40/70	425-212	90.71
2	Pantai Morib	70/140	212-106	98.42
3	Pantai Gold Coast	70/140	212-106	97.04
4	Pantai Kemasin	70/140	212-106	91.90
5	Pantai Bachok	20/40	850-425	92.75
6	Pantai Kubang Golok	40/70	425-212	90.07
7	Pantai Cahaya Bulan	20/40	850-425	90.12
8	Pantai Sabak	20/40	850-425	90.92

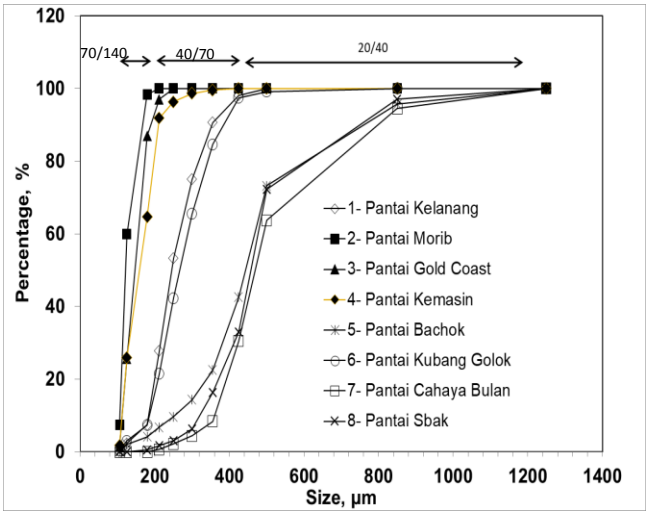

Fig. 3: Particle size distribution for all sand samples

From Table 4, only Sample 1 is within the recommended acid solubility of 2.9% (by weight) i.e. below than 3% for 70/140 mesh sizes that may due to the highest content of silica which highly resistant to acid [41]. High acid solubility of 9.6% and 8.6% in Sample 4 and 6, respectively, are due to the high content of metal oxides mineral including Fe_2O_3, Al_2O_3, CaO, MgO and K_2O which easily soluble in acid solutions [42-45]. For Sample 2 and 3 which have 70/140 mesh sizes, the acid solubility is 3.7 and 3.2% (by weight), respectively, which is slightly above the recommended value of 3% (by weight). For Sample 5, 7, 8 which are 20/40 mesh in size, the acid solubility is in the range of 2.5 -2.9%, which also slightly exceeds the recommended value of 2% by weight.

Recommended roundness and sphericity values of 0.6 or greater are desirable for sand, while 0.7 or greater are recommended to be used to produce high-strength proppants [24, 28-29]. Table 4 shows that sphericity values of all samples are greater than 0.6 while for roundness, Samples 1-3 from West Coast areas and Samples 4-8 from East Coast area showed approximately roundness of 0.5 and 0.4, respectively

Table 5 shows the results for crush values of all sand samples. Samples were subjected to five predetermined stresses and the values of fines produced were recorded. API standard requires silica sand to withstand compressive stresses of 4000 to 6000 psi before it breaks apart or ruptures. The tested size range is subjected to 4000 psi for two minutes in a uniaxial compression cylinder. API specifies that the fines generated by the test should be limited to a maximum of 20, 14, 10, and 6% by weight for 6/12, 20/40 and 16/30, 30/50 and 70/140 mesh size respectively [24, 29]. Based on the results, all samples fail to fulfil the API standard requirement since fines produced at the compressive stress is as low as 1500 psi which exceeds the maximum limit.

Table 4: General properties of all sand samples

No	Density (g/cm^3)	Turbidity (FTU)	Acid solubility (%)	Roundness	Sphericity
Recommended specifications	≥ 1.5	≤ 250	≤ 2% for 6/12-30/50 ≤ 3% for 40/70-70/140	≥ 0.6	≥ 0.6
1	1.58	176.54	2.86	0.57	0.67
2	1.42	188.65	3.67	0.58	0.65
3	1.47	164.55	3.18	0.52	0.66
4	1.40	251.45	9.56	0.43	0.72
5	1.67	162.43	2.87	0.46	0.70
6	1.48	239.74	8.65	0.45	0.72
7	1.58	300.76	2.60	0.45	0.75
8	1.54	398.65	2.55	0.46	0.72

Table 5: Crush results for all sand samples

No.	Size range	Maximum percentage fines produced at 4000 psi	% of fines produced at P (psi)				
			500	1000	1500	2000	2500
1	40/70	6	5.74	9.77	13.78	20.99	26.45
2	70/140		3.56	6.65	10.43	17.98	22.13
3	70/140		2.68	6.54	11.53	18.88	23.58
4	70/140		3.23	6.56	11.67	17.46	23.13
5	20/40	14	7.45	11.91	16.87	22.46	29.67
6	40/70	6	4.78	8.56	13.46	20.77	25.58
7	20/40	14	7.52	11.23	15.78	21.24	28.23
8	20/40		6.97	10.85	14.67	21.98	28.94

3.3. Characterization of polyurethane (PU)-coated sand

The sand from East Coast of Malaysia i.e. Pantai Bachok, Kelantan (Sample 5), was selected for coating with polyurethane. Based on the previous evaluations and characterizations, Samples 5 and 1 showed the best characteristic except that they have limitations in crush resistance, acid solubility and roundness. In this study, Sample 5 was selected because its mesh size of 20/40 that can be used as proppant material. To improve these limitations, the sand was coated with polyurethane (PU) that was synthesized from palm-based polyols. The same characterization procedure as described in Section 2.1.3 was conducted on the PU-coated sand. In this section, selected sand is noted as uncoated sand and the coated one is noted as PU-coated sand.

3.3.1. Chemical structures of Polyurethane (PU)-Coated Sand

(a) FTIR spectroscopic analysis

Figures 4 (a) and (b) show FTIR spectra of uncoated sand and PU-coated sand, respectively. Infrared (IR) spectra for Figure 4 (b) clearly indicated the formation of polyurethane by the presence of –NH frequency. An absorption peak was found between 3300 and 3350 cm^{-1} –NH carbonyl which exhibits urethane carbonyl oxygen bonds [46]. Peaks between 2926 and 2854 cm^{-1} correspond to CH bonds [47] while peak of N=C=O corresponds to asymmetric of unreacted isocyanate [48]. Common peaks for C=C, aromatic C=C and C-C bonds stretching are observed at FTIR peaks of 1656, 1594[49] and 1506 cm^{-1} respectively. Bond of H-CH is shown at the peak of 1409 cm^{-1} as stated by [47] while bands for C-O and C-N are overlapped within the range of 1350 and 1000 cm^{-1}. Although the sand was coated with PU, few peaks of Si-O-Si bond and Si-O-Si symmetric stretching were found at 1080 and 799 cm^{-1} respectively [47] for both Figures 4 (a) and (b).

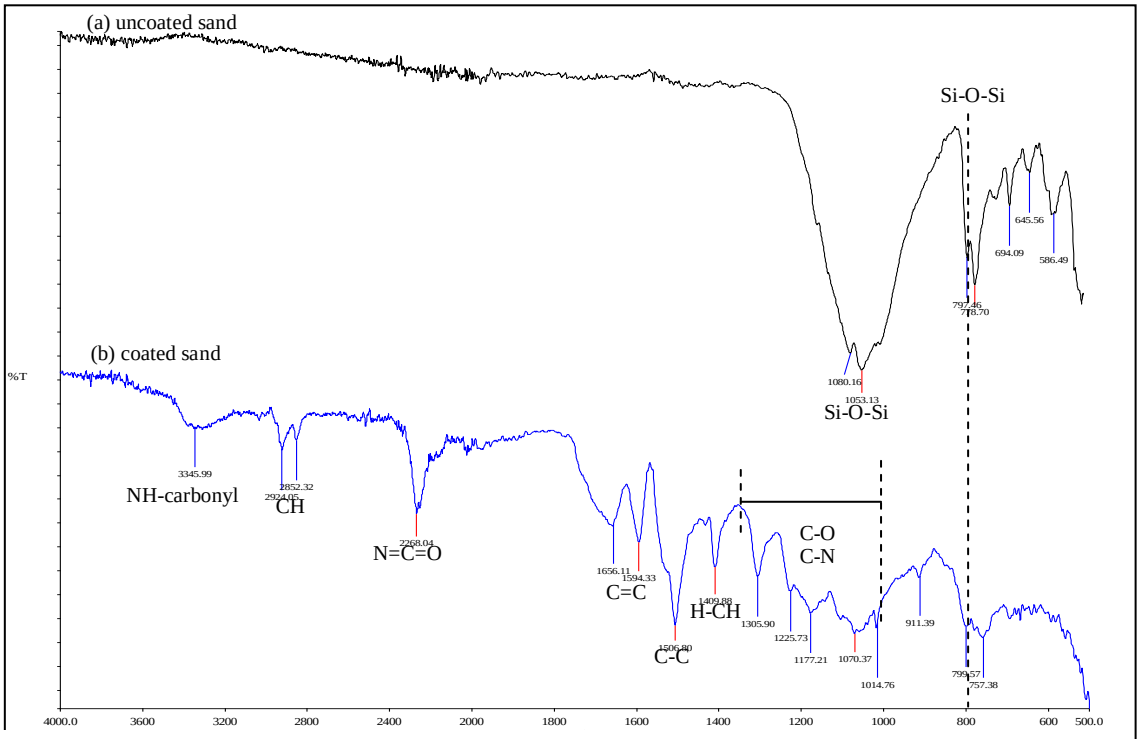

Fig.4: FTIR spectroscopic analysis of a) uncoated sand and b) PU-coated sand.

(b) Microscopic images

Figure 5 (a) and (b) show the images of uncoated and PU-coated sands, respectively, captured using digital camera while Figure 5 (c) and (d) are the microscopic images of uncoated and PU-coated sand, respectively, captured using microscope with 10 x magnification. Both samples showed different images of particle surface where the PU-coated sands are smoother, darker and more yellowish than the uncoated ones which indicate the coating of PU on the surface of the sand particles.

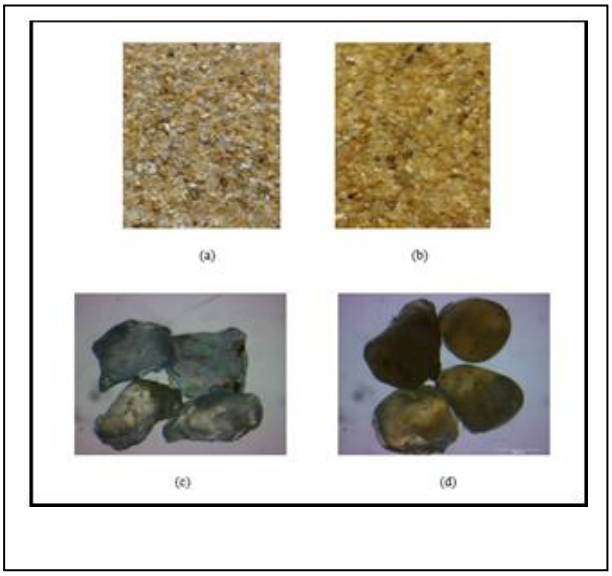

Fig.5: Camera images of (a) uncoated and (b) PU-coated sands and microscopic image of (c) uncoated and (d) PU-coated sand

3.3.2 Characterization of PU-coated sand according to API

Table 6 shows the comparison result in several characteristics between uncoated and PU-coated sand. PU-coated sand has lower bulk density and turbidity values than the uncoated sand, but the values are still within the recommended specification. Low bulk density of PU coated sand was due to the coatings that created a thin layer of polymer which is not affected the mass of the sands significantly but increased the volume of the particles. PU coating provide an impermeable barrier between proppant and external medium [21].

A tremendous improvement in acid solubility for PU-coated sand was obtained. This means that the PU coated sand did not dissolve significantly in HCl and HF solution which prevents the sand from contaminating the solutions. Previous work by [21] also showed the improvement of phenolic resin coating on proppant towards acid resistivity.

There is also improvement in the roundness and sphericity where PU-coated sand meets the API standard requirement which is 0.62 and 0.77, respectively. Thus, coating is able to help smoothing the surface of sand and form a more spherical structure. Spherical structure affected good performance and reduced production of fine particles when pressure is applied. Thus, the percentages of fines generated in crush resistance test for PU-coated sand are lower as compared with the uncoated sand (refer Table 7).

Table 7 shows crush values for uncoated and PU-coated sands. For proppant of 20/40 mesh range, API RP 56 only allows 10% by weight of fine production after 4000 psi pressure is exerted [24, 29]. PU-coated sand showed higher crush resistance compared to the uncoated sand. also stated that the crash resistance improved significantly due to resin coating. According to [21, 29, 37], angular grains tend to crush easily compared to the rounder ones as crush resistance was influenced by the particle shape of the sand. The PU-coated sand has high crush resistance due to its rounder shape and smoother surface as compared to the uncoated sands.

Table 6: Comparison between uncoated and PU-coated sand

Types	Density (g/cm^3)	Turbidity (FTU)	Acid solubility (%)	Roundness	Sphericity
Recommended specification	≥ 1.5	≤ 250	≤ 2% for 6/12-30/50 ≤ 3% for 40/70-70/140	≥ 0.6	≥ 0.6
Uncoated sand (Sample 5)	1.67	162.43	2.87	0.46	0.70
PU-coated sand	1.59	85.37	0.38	0.62	0.77

Table 7: Crush value for uncoated and PU-coated sand

Sample	% of fines produced at P (psi)							
	500	1000	1500	2000	2500	3000	3500	4000
Uncoated sand (Sample 5)	7.45	11.91	16.87	22.46	29.67	32.65	38.73	45.95
PU-coated sand	0.38	1.75	2.13	3.42	5.36	6.40	8.71	10.87

3.3.3 Impingement test of PU-coated sand

Figure 6 shows the mass loss of the targeted metal surface at different nozzle and target distance when the metal surface was impinged using both uncoated and PU-coated sands. It was found that the metal losses were less about 20-40% when the metal surface was impacted with PU-coated sand as compared to the uncoated sand. This indicates that coating can reduce the erosion of the targeted metal because the surface of the PU-coated sand should have less hardness or softer surface than the uncoated sand. The uncoated sand was assumed to be equivalent to the hardness of quartz that consists of high silica. However, the analysis on the hardness of the eroded/ impinged material was beyond the scope of this study.

Figure 6 also shows that the mass loss of targeted metal decreased as the distance between the nozzle and target increased. This is due to energy loss of the inter particles collision when the particles travelled in the gas stream. The lighter and smaller particles experienced a higher ratio of drag to inertia forces, during the interaction with the local air stream [50]. Assuming the particles experienced the same gas velocity due to the drag force, particles may experience high collision frequency at gas velocity of 100 m/s during impingement test. At this velocity, the collision frequency can be predicted to be 1,500,000 collisions/particle with approximately of collision force of 0.2 N i.e. 1000 times higher than the one predicted at gas velocity of 0.1 m/s [51]. Thus, as the particles travelled at further distance, the energy loss due to inter particle collision was also increased which reduces the impact force on the targeted metal. Hence, the impacted area produced less of mass loss with increasing of distance between the nozzle and targeted metal.

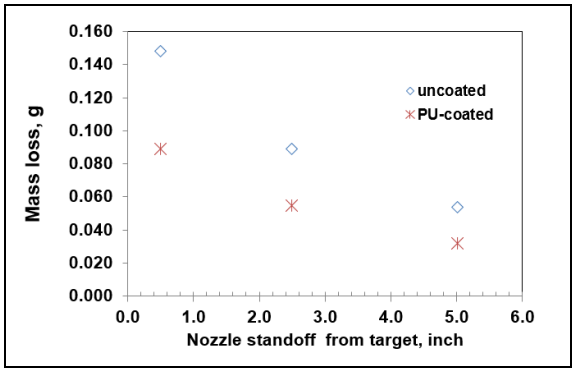

Fig. 6: Mass loss of metal target for different distance between nozzle and target.

Figure 7 shows the particle size distribution (PSD) of uncoated and PU-coated sands before and after impingement test at gas velocity of 100 m/s. The average size of the tested proppant reduced from 520 to 480 µm for PU coated sand. Whilst for uncoated sands, the average particle size reduced significantly from 520 to 380 µm after the impingement test. This confirms that PU coating reduced the attrition and fragmentation of the sand particles because flexible PU foam produced a range of compressive strength of 0.2-1.3 MPa at 10% and 25% deformations which the value varies based on the formulation [52]. Therefore, the breakage of the PU-coated sands reduced after the impingement test

Table 8 shows the images of targeted metal after being impinged by 250 g of uncoated and PU-coated sands at different nozzle and targeted metal distance of 0.5, 2.5 and 5.0 inches. The impinged areas for both types of sands, are larger and wider as the distance between nozzle and targeted metal increased because as the distances increased, the sands tend to diverge before hitting the targeted metal [53-54]. Since the breakage size of the uncoated sand reduced during the impact, most of the impacted PU-coated sand maintained at larger size compared to the uncoated ones. As for PU-coated sand, the eroded area resembled the impact of the large particles as less eroded area was observed after the impingement test [55-56]. This can be explained by the fact that larger particles which have larger ratios of inertia force and drag force compared to smaller particles, slightly change their trajectories and hit on a smaller region around the nozzle axis. Whilst, the smaller particles are diverged further from nozzle axis to the outer and hit on a larger region on the sample surface [56].

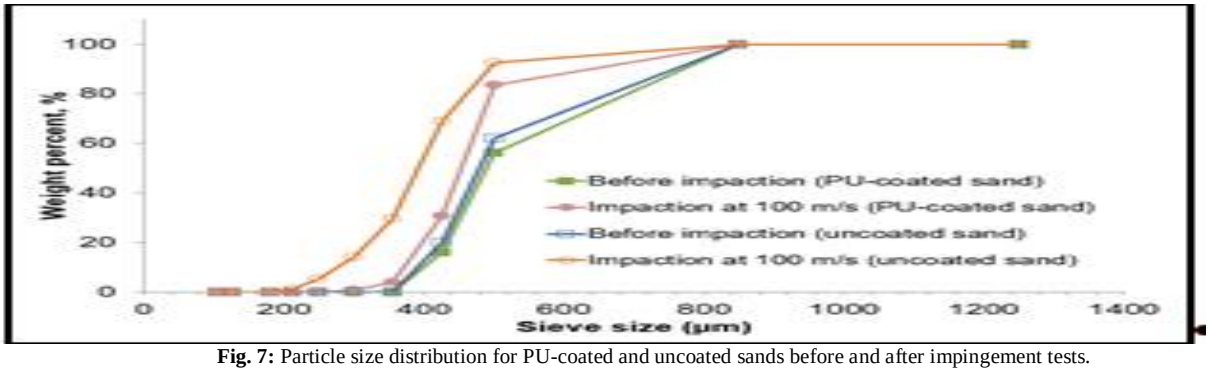

Fig. 7: Particle size distribution for PU-coated and uncoated sands before and after impingement tests.

Table 8: Images of metal on the effect of distance of nozzle and target

Distance between nozzle and target, inch	Uncoated sand	PU-coated sand
0.5	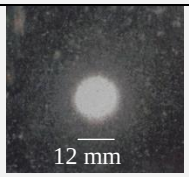	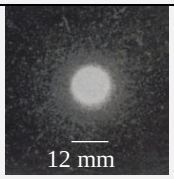
2.5	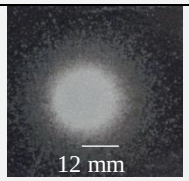	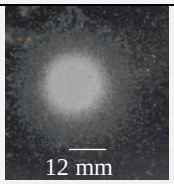
5.0	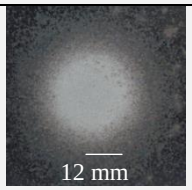	

4. Conclusion

Based on the characterization of the beach sand, it is concluded that all the samples are potential to be used as proppant with a few limitations. Sample 5 which is obtained from Pantai Bachok, (East Coast Malaysia) shows the best characteristics in terms of bulk density and turbidity but it still needs some improvement in terms of acid solubility and crush resistance. Thus, to improve its performance, it has been coated with polyurethane (PU) which was formulated from palm oil-based polyols. After coating with polyurethane, most of the characteristics of selected sand sample were improved and complied with the specifications made by API and ISO standard. PU resins treatment on sand has proven to increase its strength, reduce the acid solubility and its turbidity, where these characteristics are important for a good proppant for hydraulic fracturing. The PU-coated sand produces less impact and losses on the metal as compared with uncoated sand due to mechanical structure that provides sufficient strength to the coated surface. Furthermore, the sphericity and roundness of the PU-coated sand give less and smoother impact on the metal. Based on the overall characterization and testing, sands samples from Malaysia's beach have the potential to be used as proppant. However, the sands need to undergo coating process for further improvement to fulfill the required characteristic of proppant.

Acknowledgement

The authors gratefully like to thank Malaysian Oil Palm Board (MPOB) for the assistance and collaboration, Ministry of Higher Education (MOHE) and Universiti Teknologi MARA (UiTM) for grants of Exploratory Research Grant Scheme (ERGS) 600-RMI/ERGS 5/3 (45/2012) and Research Entity Initiative (REI) 600-RMI/DANA 5/3/REI (2/2013) respectively.

References

[1] Neto, L.B., and A. Kotousov. Residual opening of hydraulic fractures filled with compressible proppant. 2013. *International Journal of Rock Mechanics and Mining Sciences* 61: 223–230.

[2] Fink, J.K. 2013. Hydraulic fracturing chemicals and fluids technology. *Gulf Professional Publishing*. p 205

[3] Liang, F., M. Sayed, G.A. Al-Muntasheri, F.F. Chang, and L. Li. 2016. A Comprehensive review on Proppant technologies. *Petroleum* 2: 26–39.

[4] Hu, K., J. Sun, and J. Wong. 2014. Proppants selection based on field case studies of well production performance in the Bakken shale play. *SPE Conference* Paper SPE-169566.

[5] Montgomery, C.T., and M.B. Smith. 2010. Hydraulic fracturing: History of an enduring technology. *Journal of Petroleum Technology* online.

[6] Veatch Jr., R. W., and Z. A. Moschovidis. 1986. An overview of recent advances in hydraulic fracturing technology. *SPE Conference* Paper SPE-14085.

[7] Zoveidavianpoor, M., A. Samsuri, and S.R. Shadizadeh. 2012. A review on conventional candidate-well selection for hydraulic fracturing in oil and gas wells. *International Journal of Engineering and Technology* 51–60.

[8] Zoveidavianpoor, M., and A. Gharibi. 2015. Application of polymers for coating of proppant in hydraulic fracturing of subterraneous formations: A comprehensive review. *Journal of Natural Gas Science and Engineering* 24: 197–209.

[9] Parker, M.A., K. Ramurthy, and P.W. Sanchez. 2012. New proppant for hydraulic fracturing improves well performance and decreases environmental impact of hydraulic fracturing operations. *SPE Conference* Paper SPE-161344.

[10] Palisch, T., B. Wilson, and B. Duenckel. 2014. New technology yields ultra high-strength proppant. *SPE Conference* Paper SPE-168631.

[11] Youngman, R., P. R. Okell, and S. Akbar. 2002. Proppant composition for gas and oil well fracturing. US Patent US 6372678 B1, filed Sep 18, 2001 and issued Apr 16, 2002.

[12] Wu, T., and B. Wu. 2012. Corrosion resistance of ceramic proppant in BaO–CaO–P2O5–Al2O3 system. *Corrosion Sciences* 63: 399–403.

[13] Ćurković, L., M. F. Jelača, and S. Kurajica. 2008. Corrosion behavior of alumina ceramics in aqueous HCl and H2SO4 solutions. *Corrosion Sciences* 50 (3): 872–878.

[14] Wu, T., B. Wu, and S. Zhao. 2013. Acid resistance of silicon-free ceramic proppant. *Material Letters* 92: 210–212.

[15] Fang, Q., P. S. Sidky, and M.G. Hocking. 1997. The effect of corrosion and erosion on ceramic materials. *Corrosion Science* 39: 511–527.

[16] Power, G., S. C. L. Joanne, and V. Chris. 2012. Organic compounds in the processing of lateritic bauxites to alumina part 2: Effects of organics in the Bayer process. *Hydrometallurgy* 127-128: 125–149.

[17] Wu, X., Z. Huo, Q. Ren, H. Li, F. Lin, and T. Wei. 2017. Preparation and characterization of ceramic proppants with low density and high strength using fly ash, *Journal of Alloys and Compounds* 702: 442-448

[18] Zhao, J., Z. Liu, and Y. Li. 2015. Preparation and characterization of low-density mullite-based ceramic proppant by a dynamic sintering method. *Material Letter* 152: 72–75.

[19] Ma, H., Y. Tian, Y. Zhou, G. Li, K. Wang, and P. Bai. 2017. Effective reduction of sintering temperature and breakage ratio for a low-cost ceramic proppant by feldspar addition. *International Journal of Applied Ceramic Technology* 1–6

[20] Sinclair, A. R., J. W. Graham, and C. P. Sinclair. 1983. Improved well stimulation with resin-coated proppants. *SPE Conference* Paper SPE-11579.

[21] Zhang, S., L. L. C. So, S. Faucher, and L. Xi. 2016. Polymer coating over solid particles with in situ thermal curing. *Industrial and Engineering Chemistry Research* 55 (19): 5574-5584.

[22] Fu, L., G. Zhang, J. Ge, K. Liao, P. Jiang, H. Pei, and X. Li. 2016. Surface modified proppants used for proppant flowback control in hydraulic fracturing. *Colloids and Surfaces A: Physicochemical and Engineering Aspects* 507: 18-25.

[23] Cutler, R.A., and A. H. Jones. 1985. Hollow proppant and a process for their manufacture. US Patent 291,257 filed August 10, 1981, now abandoned

[24] Kaufman, P. B., H. D. Brannon, R. W. Anderson, M. A. Parker, H. D. Brannon, A. R. Neves, K. L. Abney, S. A. Joyce, M. J. Ziegler, G. W. K. P. Cortes, and G. S. Penny. 2007. Introducing new API/ISO procedures for proppant testing. *SPE Conference* Paper SPE-110697: 7.

[25] Marcovicha, N. E., M. Kuranska, A. Prociak, E. Malewska, and K. Kulpa. 2017. Open cell semi-rigid polyurethane foams synthesized using palm oil-based bio-polyol. *Industrial Crops and Products* 102: 88–96

[26] Penny, G. S. 2005. New international standards for proppant testing. *Journal of Petroleum Technology* 26.

[27] Freeman, E. R., D. A. Anschutz, J. J. Renkes, and D. Milton-Tayler. 2006. Qualifying proppant performance. *SPE Conference* Paper SPE-103623.

[28] Abney, K. 2010. Measurement of properties of proppants used in hydraulic fracturing and gravel-packing operations. Modified API RP-56 as ISO 13503-2/API RP19C. Stim-lab.

[29] Zdunczyk, M. 2007. The facts of frac. Drilling Minerals. *Industrial Minerals* 58-61

[30] Lin, X., C. Wang, J. Miyawaki, Y. Wang, S. Yoon, and I. Mochida. 2015. Analysis of the transformation behaviors of a Chinese coal ash using in-/ex-situ XRD and SEM-EXD. *Asia-Pacific Journal of Chemical Engineering* 10: 105–111.

[31] Sdiri, A. 2014. Synthesis and characterization of silica gel from siliceous sands of Southern Tunisia. *Arabian Journal of Chemistry* 7(4): 486-493.

[32] Mohd Sharif, S., N. F. Abu Bakar, and M. Nazli Naim. 2015. Deposition of fine iron oxide particles in tap water using electrophoretic deposition (EPD) technique. *Journal of Water Process Engineering* 7: 123-130

[33] Mahat, A. M., M. S. Mastuli, and N. Kamarulzaman. 2016. Influence of annealing temperature on the phase transformation of Al2O3. *AIP Conference Proceedings* 1711: 050001

[34] Wei, Z., C. Xu, and B. Li. 2009. Application of waste eggshell as low-cost solid catalyst for biodiesel production. *Bioresource Technology* 100: 2883-2885

[35] Mastuli, M.S., N. Kamarulzaman, M. A. Nawawi, A. M. Mahat, R. Rusdi, and N. Kamarudin. 2014. Growth mechanisms of MgO nanocrystals via a sol-gel synthesis using different complexing agents. *Nanoscale Research Letters* 9:134

[36] Punsuwan, N., C. Tangsathitkulchai, and T. Takarada. 2015. Low temperature gasification of coconut shell with CO2 and KOH: Effects of temperature, chemical loading, and introduced carbonization step on the properties of syngas and porous carbon product. *International Journal of Chemical Engineering* 7: 1-16

[37] Kamat, D., I. Mohd Saaid, and S. Muhammad. 2011. Comparative characterization study of Malaysian sand for possible use as proppant. *National Postgraduate Conference* (NPC).

[38] Rincón-Mora, B., M. B. Muñoz-García, J. M. Rincón, M. M. Jordán. 2017. Characterization of a locally deposited material on Arnela Beach (Galicia Coast, Spain). *Journal of Geochemical Exploration* 174: 164-171

[39] Nor, S. Z. M., R. Ismail, and M. I. N. Isa. 2012. Preliminary study on the potential of east coast of peninsular Malaysia's silica for foundry: Case Study - Terengganu. *International Journal of Material and Mechanical Engineering* 1: 53–56.

[40] Cheung, S. K. 1988. Effects of acids on gravels and proppants. *SPE Production Engineering* 3: 201–204.

[41] Abu Bakar, R., R. Yahya, and S. N. Gana. 2016. Production of high purity amorphous silica from rice husk. *Procedia Chemistry* 19: 189 – 195

[42] Cui, L., Y. Guo, X. Wang, Z. Du, and F. Cheng. 2015. Dissolution kinetics of aluminum and iron from coal mining waste by hydrochloric acid. *Chinese Journal of Chemical Engineering* 23: 590-596

[43] Fedorockov, A., and P. Raschman. 2008. Effects of pH and acid anions on the dissolution kinetics of MgO. *Chemical Engineering Journal* 143: 265–272

[44] Alkan, M., and M. Dogan. 2004. Dissolution kinetics of colemanite in oxalic acid solutions. *Chemical Engineering and Processing* 43: 867–872

[45] Jonglertjunya, W., and T. Rubcumintara. 2013. Titanium and iron dissolutions from ilmenite by acid leaching and microbiological oxidation techniques. *Asia Pacific Journal of Chemical Engineering* 8: 323–330,

[46] Kojio, K., S. Nakashima, and M. Furukawa. 2007. Microphase-separated structure and mechanical properties of norbornane diisocyanate-based polyurethanes. *Polymer* 48: 997-1004

[47] Sun, J., G. Yu, L. Liu, Z. Li, Q. Kan, Q. Huo, and J. Guan. 2014. Core–shell structured Fe3O4@SiO2 supported cobalt(II) or copper(II) acetylacetonate complexes: magnetically recoverable nanocatalysts for aerobic epoxidation of styrene. *Catalysis Science and Technology* 4: 1246–1252

[48] Peng, Y., Z. Zheng, P. Sun, X. Wang, and T. Zhang. 2013. Synthesis and characterization of polyphenol-based polyurethane. *New Journal of Chemistry* 37: 729

[49] Mohd Norhisham, S., T. I. Tuan Noor Mazneea, H. Nurul Aina, P. P. Kosheela Devi, A. Srihanuma, M. N. Norhayati, S. K. Yeong, A. H. Hazimah, C. M. Schiffman, A. Sendijarevic, V. Sendijarevic, and I. Sendijarevic. 2017. Soft polyurethane elastomers with adhesion properties based on palm olein and palm oil fatty acid methyl

ester polyols. *International Journal of Adhesion & Adhesives* 73: 38–44
[50] Macchini, R., M. S. A. Bradley, and T. Deng. 2013. Influence of particle size, density, particle concentration on bend erosive wear in pneumatic conveyors. *Wear* 303: 21-29
[51] Abu Bakar, N. F., R. Anzai, M. Horio. 2013. Microscopic evaluation of binderless granulation in a pressure swing granulation fluidized bed. *Chemical Engineering Science* 98: 51–58.
[52] Pillai, P. K. S., S. Li, L. Bouzidi, and S. S. Narine. 2016. Metathesized palm oil polyol for the preparation of improved bio-based rigid and flexible polyurethane foams, *Industrial Crops and Products* 83: 568–576.
[53] Zu, J. B., I. M. Hutchings, and G. T. Burstein. 1990. Design of a slurry erosion test rig. Wear 140 (2): 331–344.
[54] Laguna-Camacho, J. R., M. Vite-Torres, E. A. Gallardo-Hernández, and E. E. Vera-Cárdenas. 2013. Solid particle erosion on different metallic materials. In Tribology in Engineering, ed. H. Pihtili, 63-78. 1st ed. *IntechOpen*.
[55] Levy, A. V., and P. Chik. 1983. The effects of erodent composition and shape on the erosion of steel. *Wear* 1983 89(2): 151–162.
[56] Nguyen, V. B., Q. B. Nguyen, Y. W. Zhang, C. Y. H. Lim, and B. C. Khoo. 2016. Effect of particle size on erosion characteristics. *Wear* 348-349: 126–137.